

# XMM-Newton X-ray spectra of the SNR 0509-67.5: data and models

D. Kosenko<sup>1,3</sup>, J. Vink<sup>1,2</sup>, S. Blinnikov<sup>4,3</sup>, and A. Rasmussen<sup>5</sup>

<sup>1</sup> Astronomical Institute Utrecht, University Utrecht, P.O. Box 80000, 3508TA Utrecht, The Netherlands  
e-mail: D.Kosenko@astro.uu.nl

<sup>2</sup> SRON, Utrecht, The Netherlands

<sup>3</sup> Sternberg Astronomical Institute, Russia

<sup>4</sup> Institute for Theoretical and Experimental Physics, 117218, Moscow, Russia

<sup>5</sup> Stanford Linear Accelerator Center, Menlo Park, CA, USA

Received ...; accepted ...

## ABSTRACT

**Aims.** We report on X-ray observations of the supernova remnant 0509-67.5 in the Large Magellanic Cloud with XMM-Newton X-ray observatory. We use the imaging spectroscopy (EPIC) and Reflective Grating Spectrometer (RGS) data to investigate properties of the remnant and its environment.

**Methods.** The X-ray spectra were analyzed with SPEX software package. In addition to this we performed a numerical hydrodynamic simulation of the remnant.

**Results.** The EPIC data show prominent Fe K line emission, but the deduced overall amount of iron in the shocked ejecta is low. The data also show that the remnant has an asymmetric ejecta structure: the bright southwest region of the remnant shows an overabundance of metals. The analysis of the RGS spectrum shows that the remnant has a high lines velocity broadening of 5000 km/s. We found a hydrodynamical model for the remnant with basic hydrodynamical and spectral parameters similar to the observed ones.

**Conclusions.** The data analysis show that the reverse shock just recently reached iron layers of the ejecta. The brightness enhancement in the southwest region could be a sign of an asymmetric explosion or it could be the result of a density enhancement of the interstellar medium. We constructed numerical models which are in good agreement with the observations, with circumstellar density of  $3 \times 10^{-25}$  g/cm<sup>3</sup>, age of ~ 400 years, velocities of ~ 5000 km/s and an electron to ion temperature ratio of  $10^{-2}$ .

**Key words.** X-rays: individuals: SNR0509-67.5 — ISM: individuals objects: SNR0509-67.5 — ISM: supernova remnants — method: data analysis — hydrodynamics

## 1. Introduction

The X-ray emission from young supernova remnants (SNRs) provide a vital source of information about the properties of shocked, rarefied plasma, properties of the ambient medium around the remnants, and also about supernova explosion models. With the current generation of X-ray telescopes, XMM-Newton, Chandra, and Suzaku, one can combine now the imaging and spectral information to study the extended emission from SNRs. Moreover, in the case of Chandra and XMM-Newton, dispersive spectrometers allows one to obtain high resolution spectra, providing more constraints on the plasma parameters, and on the dynamics of the plasma, through Doppler shifts and broadening. The XMM-Newton Reflection Grating Spectrometers (RGS) have the advantage that the spectral quality is less deteriorated by the spatial extent of the object, at least for sources with an angular extent of  $\lesssim 1'$ .

For that reason the Large Magellanic Cloud (LMC) and the Small Magellanic Cloud (SMC) SNRs are particular well suited, since the relative proximity of the LMC means that many SNRs are bright enough to obtain high signal to noise spectra with both the CCD and grating spectrometers. On the other hand, the distance of the LMC, 50 kpc, is such that young SNRs have an extent less than  $1'$ , making them excellent targets for the XMM-Newton RGS. The XMM-Newton CCDs, with a resolution of  $\sim 6''$ , still allows one to study spatial variations, although Chandra obviously provides more spatial details. In addition, studying SMC/LMC remnants has the advantage that the interstellar absorption is on average lower than for most of the Galactic remnants, and their distance is known.

XMM-Newton observations of several LMC/SMC remnants have been published: N132D (Behar et al. 2001), 1E 0102.2-7219 (Rasmussen et al. 2001; Sasaki et al. 2006), B0540-69.3 (van der Heyden et al.

2001), N103B (van der Heyden et al. 2002), and several SMC remnants (van der Heyden et al. 2004).

Here we report on the X-ray spectrum of the SNR 0509-67.5 in the Large Magellanic Cloud. This object was already examined by several authors, e.g., Warren & Hughes (2004); Vink (2006); Badenes et al. (2008); Rest et al. (2008); Ghavamian et al. (2007); Rest et al. (2005); Badenes et al. (2007); Hendrick & Reynolds (2001). The remnant has a spherical shape and is somewhat similar in age and size to Tycho's SNR, which is also a Type Ia SNR. SNR 0509-67.5 has an angular diameter of  $25''$ , corresponding to the radius of 3.6 pc (Warren & Hughes 2004). A recent analysis by Rest et al. (2005), based on light echo detection, and Badenes et al. (2008), based on modeling of the X-ray observation, suggest the age of the remnant to be  $\sim 400$  years. Estimates by Ghavamian et al. (2007) gives the values of 295 – 585 years, consistent with the rough estimate  $\sim 500$  years by Vink (2006), based on a preliminary analysis of the XMM-Newton data.

A detailed analysis of the X-ray emission of SNR 0509-67.5 was made by Warren & Hughes (2004) and based on Chandra X-ray data. Their study revealed that the remnant is rich in silicon, sulfur and iron, the bulk of the continuum emission has a non-thermal origin, and an estimate the circumstellar medium (CSM) density is of  $\sim 0.05 \text{ cm}^{-3}$ . The preferred model for the explosion which produced the remnant — is delayed detonation.

Recently, Badenes et al. (2008) reported their study of the remnant's X-ray spectrum observed by Chandra and XMM-Newton observations. They performed hydrodynamical and X-ray spectral calculations of the remnant and concluded that it was an energetic, delayed detonation explosion of  $1.4 \times 10^{51}$  ergs with a nickel mass of  $0.97 M_{\odot}$ . In their numerical simulations the circumstellar density was set to  $n_{\text{CSM}} = 0.4 \text{ cm}^{-3}$  and the ratio of electron to ion temperatures to 0.02.

For illustrative purposes we show in Fig.1 some of the Chandra X-ray images of the remnant in three different bands. The overall structure of the SNR shows a large scale inhomogeneity in the shell. The Southwest (SW) part of the remnant is somewhat brighter compared to the average brightness.

In the current study we performed an analysis of the remnant employing XMM-Newton X-ray observations and SPEX fitting software (Kaastra et al. 1996). We also performed hydrodynamical simulations of the SNR 0509-67.5, employing the hydrocode SUPREMNA (Sorokina et al. 2004) to compare numerical predictions for the remnant with the observations.

The paper is organized as follows. First we describe briefly the XMM-Newton data in §2, then we discuss the X-ray spectrum in §3. Numerical models for the SNR are presented in §4. We discuss our results and outline them in §5.

## 2. The XMM-Newton data, reduction and analysis

SNR 0509-67.5 was observed with the XMM-Newton X-ray Observatory (obs ID 0111130201) for 35.9 ks on July 4, 2000. The observatory contains three X-ray telescopes. Behind all of them are CCD detectors, collectively called the European Photon Imaging Camera (EPIC). Two of them are MOS type CCD detectors called MOS1 and MOS2 (Turner et al. 2001), the other is of the pn-CCD type (Strüder et al. 2001). The telescopes equipped with MOS CCD detectors in the focal plane contain also the Reflective Grating Spectrometers (RGS), consisting of the Reflective Grating Arrays, dispersing about 50% of the X-rays to two CCD arrays (den Herder et al. 2001). XMM-Newton observations therefore provide simultaneous data from all five X-ray instruments: the two MOS-CCDs, the pn-CCD, and the two RGS instruments.

In this paper we concentrate on the data obtained with the MOS detectors and the RGS. Although the EPIC-MOS have a somewhat lower sensitivity than the EPIC-pn instrument, they have better spectral resolution, which is important for line rich sources, such as SNRs.

Note that Badenes et al. (2008) found an inconsistency between EPIC MOS1,2 and PN spectra. They investigated Si  $K_{\alpha}$  line centroid location in the datasets of these devices and found out that the line centroids of MOS and PN detectors are shifted with respect to each other. The authors rejected MOS1 and MOS2 data and concentrated only on the Chandra and EPIC-pn spectra. We confirm this inconsistency: analysis of the Si  $K_{\alpha}$  centroid of MOS1,2 and PN data reveals that it is located at  $1.8503 \pm 0.0012 \text{ keV}$  and  $1.8298 \pm 0.0015 \text{ keV}$  respectively (the errors are  $1\sigma \chi^2$ ). For the Fe  $K_{\alpha}$  line we found  $6.495 \pm 0.048 \text{ keV}$  and  $6.442 \pm 0.025 \text{ keV}$ . The discrepancies in the lines locations are about 1%. Nevertheless, there are indications, that PN instrument has small gain problems and sometimes a shifting of the PN energy grid is required (private communications with N.Werner; Werner et al. 2006; de Plaa et al. 2004). Moreover, in our study, we were unable to find a fitting model with sensible parameters of the emitting plasma for the PN data, meanwhile a spectral model for the MOS data gives reasonable and satisfactory plasma parameters.

The EPIC data was slightly affected by background flaring ("soft protons"). As a result we cut out 3.4 ks of the total observation. The MOS1 observation was done in small window mode, whereas the MOS2 data were made in full frame mode. For MOS1, therefore, we could not select a region to extract background spectra. For the MOS2 this was possible, but we found that the background correction was too small, and the account for it did not change the fitted parameters. For that reason we did not include background subtraction for our final analysis.

The RGS is a slitless spectrometer. For an extended source this means that the spectrum is smeared by the image of the source itself. For SMC/LMC remnants the smearing is modest, but present, and it gives rise to

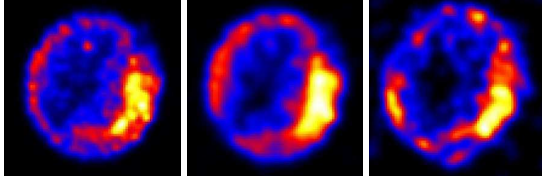


**Fig. 1.** Chandra images of the SNR 0509-67.5 in different X-ray ranges. From left to right: 0.45-1.75 keV, 1.8-2.5 keV, 2.5-6.0 keV (Warren & Hughes 2004).

a change in the line spread function. For our analysis we incorporated this effect into the response matrix by convoluting the standard (point source) response matrix with the emissivity profile of the SNR, as obtained from archival Chandra observations. This procedure was also for the RGS data of SN 1006 (Vink et al. 2003). As we shall show later, however, in the case of 0509-67.5 the Doppler line broadening is much larger than broadening due to the spatial extent of the remnant.

Apart from adapting the RGS response matrix, all reduction for both MOS and RGS data was done using the standard XMM-Newton software package SAS version 7.1.0.

### 3. Spectral models

The X-ray spectra of the SNR were fitted with a non-equilibrium ionization (NEI) model, which is a part of the SPEX fitting package (Kaastra et al. 1996). The package does not include a plane shock model (which takes into account temperature and ionization timescale gradients), but it contains the most complete and up-to-date set of atomic data. The use of a single ionization timescale NEI model is justified in some cases, when one needs to get rough estimates of basic SNR properties (e.g. Cassam-Chenaï et al. 2004). The emission measure  $n_e n_H V$  in such a model can be used to estimate the circumstellar medium density. Since continuum emission stems mostly from the shocked CSM, the value of  $n_H$  can give us directly an estimate of the unshocked environment density (depending on the assumed equation of state).

Combined fitting of the spectra from RGS, EPIC: MOS1, MOS2 devices is presented in Fig.2.

#### 3.1. EPIC data

##### 3.1.1. Spectra parameters

In order to adequately fit the spectra we needed at least two thermal components: one NEI component is for the bulk of the X-ray line emission, and another one is to fit the Fe-K emission around 6.5 keV (see section 3.1.2 for details on this component). We also investigated a model with an additional power law continuum, since Warren & Hughes (2004) reported indirect evidence for non-thermal continuum, probably synchrotron emission from  $> \text{TeV}$  electrons. The plasma parameters for the

two models are indicated in Table 1 as (th) and (th+pow). In addition, we extracted also the spectrum from the enhanced SW region of the remnant. In general, the parameters are in agreement with the ones obtained by Warren & Hughes (2004). The enhanced SW region shows higher ionization timescale, probably reflecting a higher density.

Using the value of the emission measure, we can estimate the density of the CSM. Hydrogen emission measure (Table 1, MOS+RGS) is  $EM = n_e n_H V = 1.5 \times 10^{58} \text{ cm}^{-3}$  and the remnant's size is  $R = 3.6 \text{ pc} \approx 10^{19} \text{ cm}$ . Assuming that the emitting shell has a width of  $\Delta R = R/12$ , so that the volume  $V_X = V_{tot}/4 = \pi R^3/3 \approx 10^{57} \text{ cm}^3$ , we obtain  $n_e n_H \approx 15 \text{ cm}^{-6}$ . Furthermore, assuming that all the matter is ionized  $n_H \approx 4 \text{ cm}^{-3}$ , we obtain that CSM number density for the remnant should be  $n_{CSM} \approx 1 \text{ cm}^{-3}$  for the neutral circumstellar environment, which appears to be the case for SNR 0509-67.5 (Ghavamian et al. 2007). Here we assumed shock compression ratio to be 4 for non-relativistic matter with adiabatic index  $\gamma = 5/3$ . However, cosmic ray (CR) acceleration may play an important role in SNR dynamics. For a cosmic ray dominated shock the adiabatic approach that of a relativistic gas ( $\gamma = 4/3$ ) gives rise to a compression factor of 7. Cosmic ray escape may even increase the compression ratio beyond 7 (Berezhko & Ellison 1999). Tycho's SNR provides some observational evidence for high compression factors (Warren et al. 2005). Therefore, in the case of 0509-67.5, the pre-shock density could be as low as  $n_{CSM} \lesssim 0.6 \text{ cm}^{-3}$ .

Also, two additional sources of uncertainty concerning the pre-shock density are the presence or absence of a non-thermal continuum, and chemical composition. In particular, our above estimate assumes that most of the continuum is bremsstrahlung from hydrogen-electron collisions, whereas it is quite likely that parts of the remnant consist of pure metal plasmas, in which case bremsstrahlung comes from metal ions and the electrons they provide, in general this lowers the density estimate. Therefore, our estimate of  $n_{CSM} \approx 1 \text{ cm}^{-3}$ , should be considered as an upper limit.

Abundances of chemical elements for the entire SNR (thermal and nonthermal continuum) and enhanced SW part for the simple NEI model are presented in Fig.3. Abundances for some theoretical explosion models (Iwamoto et al. 1999; Woosley et al. 2007) are also shown. The accounting for the nonthermal continuum does not create a considerable difference in the abundances set, but naturally it makes the remnant more metal-rich. One can see from the figure that the SW region is more metal abundant compared to overall remnant values (2-3 times higher amount of metals).

The SPEX fitting shows no evidence for interstellar absorption, which means that the value of  $N_H$  is low for this remnant. The column density value found by Warren & Hughes (2004) is  $N_H \approx (5 - 9) \times 10^{20} \text{ cm}^{-2}$ . Which is, indeed, the lowest value among all known LMC supernovae remnants (Hughes et al. 1998). This could

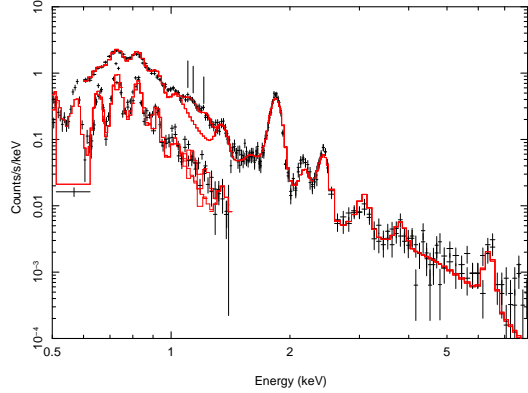


**Fig. 2.** MOS1, MOS2 and RGS data fitted with the NEI model, the Fe K line is fitted separately: a NEI component with  $kT = 3.5$  keV and  $n_e t = 10^9$  s/cm<sup>3</sup>. Vertical lines show the location of three Gaussians, which substitute missing in SPEX model Fe L lines (the energies are 1.102, 1.125 and 1.226 keV).

suggest that the remnant is located on the near side of the LMC.

The power law model for the continuum gives a value for the nonthermal flux of  $F_{1keV}^X = (2.3 \pm 0.3) \times 10^{-4}$  ph/s/cm<sup>2</sup>/keV with power index of  $\Gamma = 3.5 \pm 0.1$ , which is steeper than expected for this kind of remnants, e.g. Tycho SNR (c.f. Tycho's SNR or Cas A Cassam-Chenaï et al. 2006; Vink & Laming 2003). This value is close to the one obtained by Warren & Hughes (2004):  $3.25 \pm 0.18$ . The extrapolation of the non-thermal radio flux (Hendrick & Reynolds 2001) to the X-ray range yields  $F_{1keV} = 1.4 \times 10^{-2}$  ph/s/cm<sup>2</sup>/keV. Since the X-ray synchrotron spectrum is likely to be affected by synchrotron losses, this flux should be considered as an upper limit.

### 3.1.2. Fe-K emission

Despite of the low amount of iron in the shocked ejecta deduced with single ionization timescale NEI model, the spectrum has a pronounced Fe K feature. Its centroid is located at  $6.50 \pm 0.05$  keV, which may correspond to the ions from Fe VII (Kaastra & Mewe 1993) with  $n_e t \approx 10^9$  s/cm<sup>3</sup> up to Fe XVII with  $n_e t \lesssim 10^{10}$  s/cm<sup>3</sup>. We fitted the Fe K line separately with the temperature  $kT = 3.5$  keV and ionization timescale  $n_e t = 10^9$  s/cm<sup>3</sup>. The ionization time is uncertain, but it is impossible to fit the Fe K emission with a component with  $n_e t > 2 \times 10^9$  s/cm<sup>3</sup>, since then the spectrum would have exhibited much more Fe L emission than observed. Given the low  $n_e t$  it is likely that the Fe K emission is associated with pure Fe, recently shocked by the reverse shock.

The separate fitting of the Fe K feature allows us to make a crude estimate of the amount of swept up iron layer of the supernova ejecta. Assuming that the pressure

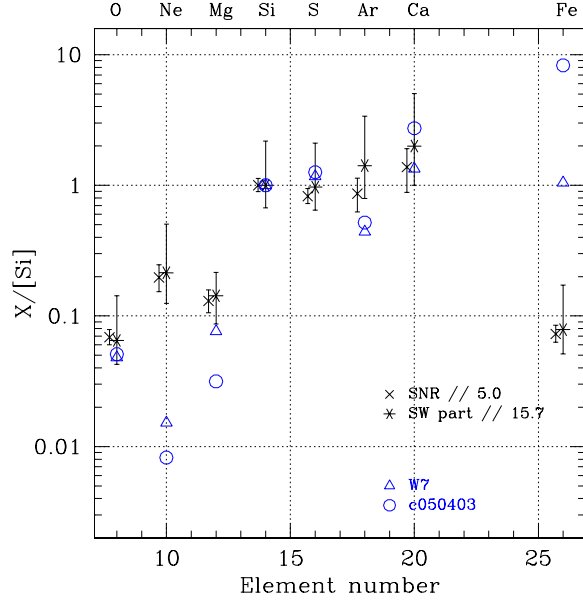


**Fig. 3.** Abundances of the entire remnant and its SW region, obtained in fitting of the EPIC (MOS1 and MOS2) spectrum. Abundances for the classical W7 (Iwamoto et al. 1999) and for the delayed-detonation model c050403m (Woosley et al. 2007) are also shown. Theoretical abundances are taken from numerical simulations (described below) include swept up ( $\sim 0.7 M_\odot$ ) ejecta and shocked LMC circumstellar medium. All abundances are solar normalized. Errors are  $1 \sigma$  rms. The silicon abundance (with respect to solar) for the entire SNR is 5.0 and for the SW part of it is 15.7.

and temperature do not change drastically throughout the shell, and thus the electron density  $n_e$  remains approximately constant, we can employ the following relation  $n_{Fe} V_{Fe} \sim (EM_{Fe}/EM_X)(n_H V_X)$ .

The value of the emission measure of the pure iron NEI component,  $EM_{Fe} = n_e n_{Fe} V_{Fe} \approx 4 \times 10^{54}$  cm<sup>-3</sup>, basic NEI component,  $EM_X = n_e n_H V_X \approx 10^{57}$  cm<sup>-3</sup>, and also the density  $n_H \approx 4$  cm<sup>-3</sup> and the volume  $V_X \approx 10^{57}$  cm<sup>3</sup> of the emitting shell, yield us the estimate of the swept up iron in the remnant of  $M_{Fe} = 56 m_U n_{Fe} V_{Fe} \sim 0.05 M_\odot$  (with  $m_U = 1.66 \times 10^{-24}$  g,  $M_\odot = 2 \times 10^{33}$  g). This is less than 10% of the iron amount in a typical Ia SN model (Nomoto et al. 1984; Iwamoto et al. 1999).

### 3.1.3. The line emission deficit around 1.2 keV

The EPIC (MOS1,2) models do not fit an excess of emission around 1.2 keV. This feature is also present in the EPIC-pn spectra, and is weakly visible in the RGS spectra. Therefore, this excess is likely to be real and not caused by calibration errors or background features. It is possible to fit this region of the spectrum, but only if we allow for unrealistic overabundances of either Na (approximately 5 times of Si) or Ni (4 times of iron).



**Table 1.** Parameters for the SNR 0509-67.5 (last column contains data for the southwest region), EPIC (MOS1,2) and RGS data. Errors are 1 sigma ( $\chi^2$ -distribution). th — basic (single ionization timescale) NEI model, th+pow — NEI with power-law continuum.

Parameter	th, MOS+RGS	th, MOS	th+pow, MOS+RGS	th+pow, MOS	SW, th, MOS
$n_e n_H V \times 10^{58}, \text{ cm}^{-3}$	$1.15^{+0.12}_{-0.12}$	$0.98^{+0.10}_{-0.10}$	$0.55^{+0.15}_{-0.16}$	$0.95^{+0.11}_{-0.10}$	$0.07^{+0.05}_{-0.04}$
$kT, \text{ keV}$	$4.01^{+0.23}_{-0.18}$	$5.02^{+0.33}_{-0.28}$	$4.55^{+0.22}_{-0.20}$	$4.98^{+0.30}_{-0.30}$	$4.59^{+0.54}_{-0.45}$
$n_e t \times 10^{10}, \text{ s/cm}^3$	$1.41^{+0.03}_{-0.03}$	$1.62^{+0.05}_{-0.05}$	$1.63^{+0.04}_{-0.04}$	$1.60^{+0.05}_{-0.06}$	$1.52^{+0.08}_{-0.08}$
$\sigma_v, \text{ km/s}$	$6030 \pm 170$	$5700 \pm 220$	$5050 \pm 180$	$5350 \pm 240$	$6100 \pm 500$
$\chi^2/d.o.f.$	2.61	1.42	2.29	1.37	1.66

In our view the possible cause is the uncertainty in the atomic data base of SPEX concerning the Fe-L emission. The Fe-L emission of SNR 0509-67.5 is dominated by Fe XVII emission. So it is likely that the excess is due to incompleteness of the atomic database concerning Fe XVII, in particular due to line emission from the  $n = 4$  to  $n = 2$  level. This is corroborated by the fact that the series limit of Fe XVII is at 1.26 keV, which also roughly marks the end of the emission excess. Some  $n = 4 \rightarrow 2$  lines are present in the SPEX code, but their emission strengths may be underestimated. This may not be surprising, since the code has been tested primarily on collisional equilibrium sources, whereas in NEI  $n = 4 \rightarrow 2$  may be enhanced due to non-equilibrium effects, such as inner shell ionization of Fe XVI.<sup>1</sup>

### 3.2. RGS data

The high resolution RGS spectra allowed us to evaluate the velocity broadening of the X-ray emission lines and make an independent estimate of the CSM density. Thus, from the spectrum in energy range of 0.3 – 2.5 keV we find  $\sigma_v = 4900 \pm 420$  km/s (which is the preferred value since it is based on the RGS only). This gives us an upper limit on the age of the SNR of  $t \lesssim R/v_{\text{shock}} \approx 540 \pm 50$  yr (assuming  $v_{\text{shock}} = 4/3\sigma_v$ ).

The first column in Table 1 shows the best fit parameters for the joint MOS+RGS analysis. However, we also fitted the RGS spectra separately with a single NEI model. In this case the fitted parameters are quite different, in particular the plasma temperature:  $kT_e = 0.75^{+0.33}_{-0.09}$  keV and ionization timescale  $n_e t = (1.28^{+0.25}_{-0.33}) \times 10^{10}$  s/cm<sup>3</sup>. The probable reason is that the RGS is mostly sensitive to the energies in 0.5-1 keV, so it misses the contribution from lines that mostly emit at higher temperatures and the continuum. In particular the OVII lines around 0.55 keV/22 Å has much more statistical weight in the

RGS spectra. The OVII line emission probably has contributions from a lower temperature plasma, that is not picked up by the MOS spectra. The discrepancy therefore points to the presence of temperatures gradients in the SNR.

Ideally, one would like to incorporate those gradients into a more complete model of the X-ray emission from SNR 0509-67.5. We made an attempt to obtain such a model by fitting a joint MOS-RGS model with 3 NEI components, one for the low temperature plasma, one for the bulk of the MOS spectrum, and one for the Fe-K line emission. However, it turned out to be difficult to come up with a unique, satisfying solutions, given the complexity of the parameter space. Moreover, it would still involve some arbitrary choices. For example, it is not clear what to do with the abundances; assume one set of abundances for the first two NEI components, but then we do not allow for possible abundance gradients that are also likely to be present. So in short, we have reached here the limit of what is possible with multiple components. The RGS data, however, do show that the models in Table 1 are incomplete.

One of the advantages of the high spectral resolution of the RGS is that it is possible to obtain an estimate of the nitrogen abundance. Nitrogen is not an ejecta product of Type Ia supernovae, so any nitrogen must come from the shocked CSM. Therefore, the nitrogen abundance, together with the emission measure makes it possible to obtain an alternative estimate of the pre-shock CSM density, avoiding some of the confusion due to mixture of pure metal, ejecta components.

The hydrogen emission measure of the RGS fit is of  $n_e n_H V = 4 \times 10^{59}$  cm<sup>-3</sup> and emitting volume of  $V_X \approx 10^{57}$  cm<sup>3</sup> yield  $[n_e n_H]^{\text{RGS}} \approx 400$  cm<sup>-6</sup>. Taking into account best-fit RGS amount of nitrogen  $X_N^{\text{RGS}} = 0.01$  and typical LMC abundance  $X_N^{\text{CSM}} = 0.4$  (both in solar units), we derive for the circumstellar matter  $[n_e n_H]^{\text{CSM}} = [n_e n_H]^{\text{RGS}} (X_N^{\text{RGS}}/X_N^{\text{CSM}}) = 10$  cm<sup>-6</sup>. Thus for the shocked CSM (LMC abundances)  $n_H = 3$  cm<sup>-3</sup>, which yields  $n_{\text{CSM}} = 0.4 - 0.8$  cm<sup>-3</sup>.

<sup>1</sup> We discussed this issue with Dr. Kaastra, one of the authors of the SPEX code, who agrees that this may explain the lack of a good fit around 1.2 keV.

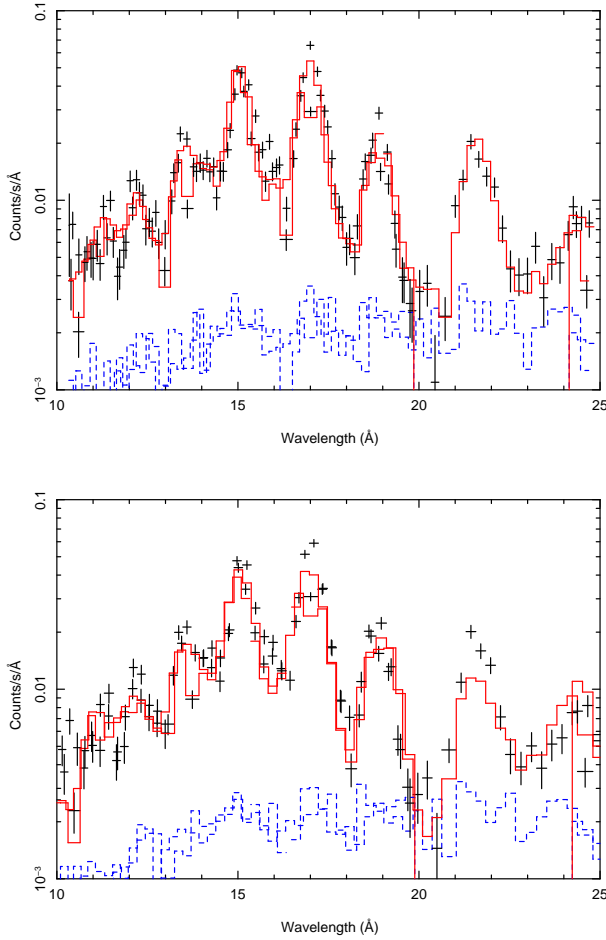


**Fig. 4.** Top: the RGS spectra with best-fit NEI model. Bottom: the RGS spectra and the MOS+RGS best-fit NEI model.

#### 4. Numerical models

To simulate the evolution of the remnant and to compare it with the observed data, we employed the hydrodynamical code SUPREMNA, which is explained in details in Sorokina et al. (2004). The code assumes spherical symmetry, but it incorporates many relevant physical processes, without which it is not possible to accurately predict peculiarities of SNR radiation, such as time-dependent ionization, inner-shell collisional ionization, possible difference in temperatures of electrons and ions, the influence of radiative losses, the account of electron thermal conduction and nonthermal particles. The calculations of the lines emission was based on Gaetz & Salpeter (1983) and Mewe et al. (1985). The introduction of inner-shell ionization processes is described in Kosenko (2006).

To reproduce the observed remnant in numerical simulations we considered various physical conditions of the CSM and also different explosion models: deflagration —

W7 (Nomoto et al. 1984) and some of the ‘mildly-mixed’ delayed-detonation models (Woosley et al. 2007).

Following the estimates of the CSM density derived from the SPEX spectral fitting, we surround the remnant with uniform medium of  $\rho_{\text{CSM}} = 3 \times 10^{-25} \text{ g/cm}^3$ . In this set up we found that at the age of  $t \sim 400$  years the modeled remnant’s radius reaches  $R \sim 3.6 \text{ pc}$ , with typical velocities of the plasma of  $v \sim 5000 \text{ km/s}$ . These parameters are in agreement with the observed ones of the SNR 0509-67.5. Modeled temperatures and X-ray spectra will be discussed in details below.

##### 4.1. Basic modeling

First, we used a ‘‘basic’’ approach, described in Sorokina et al. (2004) where electrons and ions are being heated partially due to artificial viscosity and degree of the electrons heating is controlled by a parameter  $q_i$ , such that  $P_i = P_i(\text{thermal}) + q_i Q$  and  $P_e = P_e(\text{thermal}) + (1 - q_i) Q$ , where  $P_e$ ,  $P_i$  — electrons and ions pressure,  $Q$  — artificial viscosity (is the case when only collisional energy exchange takes place  $q_i = 1 - m_e/m_i$ ,  $m_e$ ,  $m_i$  — electron and ion masses). Note that since  $q_i$  controls the efficiency of electrons heating (their temperature may vary theoretically from  $10^{-4} T_i$  to  $T_i$ ), this parameter has a strong influence on the X-ray spectrum behavior (line fluxes with respect to free-free continuum).

In this framework we have found that the best fit (in terms of  $\chi^2/d.o.f.$ ) for the observed spectrum gives the value of  $q_i = 0.99$ , which yields the typical ratio of  $T_e/T_i \approx 3 \times 10^{-3}$  for the case of W7 explosion model. We also considered a library of thermonuclear explosion models by Woosley et al. (2007). We employed several of them with various amounts of iron and intermediate mass elements (IME). We have found that the explosion of a ‘‘mildly-mixed’’ delayed detonation model with  $E = 1.4 \times 10^{51} \text{ ergs}$ ,  $M_{\text{Ni}} = 0.5 M_{\odot}$ ,  $M_{\text{Fe}} = 0.4 M_{\odot}$ ,  $M_{\text{IME}} = 0.3 M_{\odot}$  (c050403m model in Woosley et al. 2007, notation) gives the best-fit to the observed EPIC MOS spectrum of the SNR with  $q_i = 0.9$  and thus  $T_e/T_i \approx 3 \times 10^{-2}$ . These values seem to be in reasonable agreement with the relation  $T_e/T_i \propto v_S^{-2}$  ( $v_S$  — shock velocity) proposed by Ghavamian et al. (2000). Indeed, assuming for the SNR 0509-67.5 shock front speed of  $v_S \approx 4/3v \approx 6000 \text{ km/s}$ , according to Ghavamian et al. (2000, Fig.2) we should expect  $T_e/T_i = 6 \times 10^{-3}$ .

The simulated (for these two explosion models) and the observed X-ray spectra are presented in Fig.6. Note that all of our models exhibit noticeable lack of flux in the region of Fe L complex (compared to the observed spectrum). This is caused by some incompleteness of the atomic data set for Fe L emission employed in our package, as verified by directly comparing a single NEI model as obtained by the SUPREMNA code and in SPEX. This issue will be addressed in future updates of the SUPREMNA code.

At higher densities of the CSM, there is no the Fe L emission deficit, but in these models the expansion rate of the shell and the radius of the contact discontinuity are in

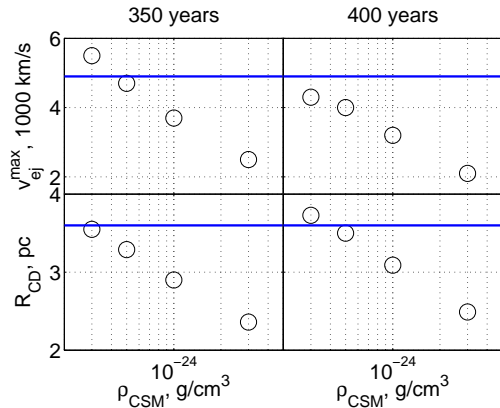


**Fig. 5.** Maximum velocity of the shocked ejecta ( $v_{ej}^{max}$ , upper row) and position of the contact discontinuity ( $R_{CD}$ , lower row) depending on the value of CSM density for 350 (left column) and 400 years (right column). Explosion model — delayed detonation c050403 (Woosley et al. 2007) with  $E = 1.4 \times 10^{51}$  ergs. The observed values of the velocity and radius of the remnant are also outlined.

disagreement with the observed values of the lines broadening and the remnant’s size. So the value of CSM density was chosen to satisfy the observed velocity of the emitting ejecta, the age and the geometrical size (assuming that the observed edge of the remnant close corresponds to the location of the contact discontinuity) of the remnant for the considered explosion mechanisms. Figure 5 shows maximum velocity of the shocked ejecta and position of the contact discontinuity depending on the assumed value of CSM density for the delayed detonation explosion model c050403 at the age of 350 (left panels) and 400 (right panels) years. The figure indicates that for an assumed age of 400 years, the CSM density of  $3 \times 10^{-25}$  g/cm<sup>3</sup> gives a reasonable compromise between velocity and radius. An assumption that the remnant may be as young as 350 years, allows the CSM to be denser than  $5 \times 10^{-25}$  g/cm<sup>3</sup>, but in this case the synthetic X-ray spectra disagree with the observed ones (there are major discrepancies in Fe L emission and Si K and S K lines fluxes). More energetic ( $E > 1.4 \times 10^{51}$ ) progenitor could shift the allowable values of the density to higher ranges. We checked several of them, which contain more  ${}^56Ni$ , and which could be consistent with the optical spectrum of the supernova, as extracted from the light echo (Rest et al. 2008). However, these models contain too little Si and S to fit their emission lines.

X-ray spectra of the simulated and the observed (merged MOS1 and MOS2, crosses) remnants. The theoretical spectra are based on W7 ( $T_e/T_i \approx 0.003$ ,  $\chi^2/d.o.f. \approx 27$ , dashed line) and delayed-detonation c050403m ( $T_e/T_i \approx 0.03$ ,  $\chi^2/d.o.f. \approx 19$ , solid line) explosion models,  $\rho_{CSM} = 3 \times 10^{-25}$  g/cm<sup>3</sup>, age  $t = 400$  years.

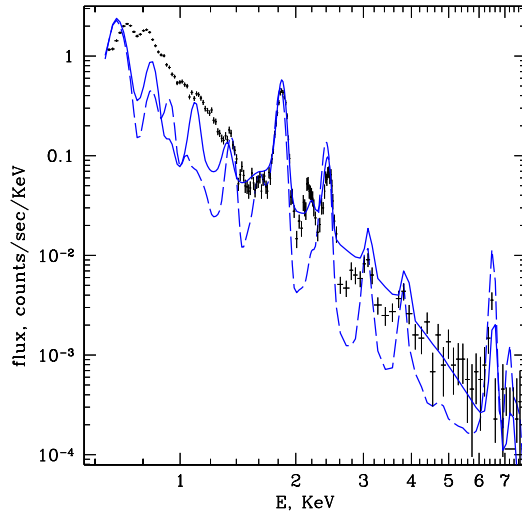


**Fig. 6.** X-ray spectra of the simulated and the observed (merged MOS1 and MOS2, crosses) remnants. The theoretical spectra are based on W7 ( $T_e/T_i \approx 0.003$ ,  $\chi^2/d.o.f. \approx 27$ , dashed line) and delayed-detonation c050403m ( $T_e/T_i \approx 0.03$ ,  $\chi^2/d.o.f. \approx 19$ , solid line) explosion models.  $\rho_{CSM} = 3 \times 10^{-25}$  g/cm<sup>3</sup>, age  $t = 400$  years.

The Table 2 shows a list of some basic properties of these models. Some of the numerical values in the table are upper limits or just typical for the corresponding case. Errors are presented where appropriate.

#### 4.2. Accounting for the cosmic rays

We introduced an additional component representing the pressure and energy from (relativistic) cosmic ray particles, in a way that could be easily implemented within the current framework of this code. This was done by altering (softening) the equation of state as follows:

$$\begin{cases} P = P_g + \frac{1}{3}\hat{a}T^4 \\ E = E_g + \hat{a}T^4 \end{cases} \quad (1)$$

where  $P_g$  is the gas pressure,  $E_g$  is the gas internal energy,  $T$  is the “temperature” and  $\hat{a}$  is a free parameter mimicking the contribution of the relativistic particles. Effectively it means, that some part of the energy is transferred into relativistic particles, which behave similar to a photon gas.

Density profiles for the cases with and without this relativistic correction for the delayed-detonation c050403m (Woosley et al. 2007) model are presented in Fig.7. Note that in the case of the relativistic alteration of the equation of state (gray solid line), the density jump at the forward shock is enhanced, compared to the basic set up. The density profile of the ejecta behind the reverse shock became affected as well.

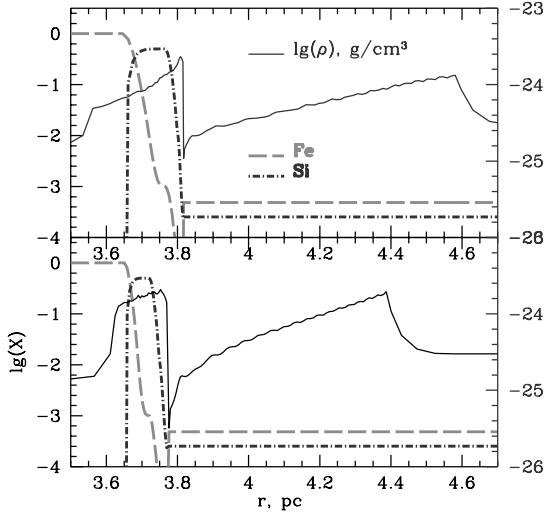


**Fig. 7.** Density profiles (solid lines) against radius for the hydrodynamical models of age 400 years and for the delayed detonation explosion mechanism c050403m. Upper panel: basic set up, lower panel: the set up with the relativistic correction in the equation of state (Eq. 1). Also the distributions of Si (black dash-dotted line) and Fe (gray dashed line) in the ejecta are shown.

However, in reality the cosmic ray contribution to the internal energy may be different for the forward and reverse shock. Recently, Helder & Vink (2008) established, that in the case of the SNR Cas A, the reverse shock can accelerate cosmic ray particles up to energies of a few TeV.

In this set up, a configuration with the cosmic-ray energy density  $E_{CR} = \hat{\alpha}T^4$  of the order of  $0.4E_g$ , produce a model which also gives a good fit to the observed spectrum. The modeled and observed X-ray spectra for this approach are presented in Fig.8.

Chevalier (1983) considered self-similar solutions for a mixture of a fluid with  $\gamma = 5/3$  and a relativistic gas (i.e., cosmic rays) with  $\gamma = 4/3$ . The effective adiabatic index was determined by a constant fraction of cosmic rays in total pressure. Later Blondin & Ellison (2001) used a constant value of effective  $\gamma$  which was taken sometimes even lower than  $4/3$  to allow for a stronger compression ratio mimicking radiative shock waves. We note that our parametrization, being also simple in comparison with a true cosmic rays model, is much richer than used by Chevalier (1983); Blondin & Ellison (2001) in their purely hydrodynamic studies. We do not assume a constant fraction of cosmic rays or a constant value of effective  $\gamma$ , thermal conduction and radiative losses are fully included into a hydrodynamical scheme, in contrast with the vast majority of modern work on the subject. However, the validity of our simplified model of cosmic ray contribution requires further tests and compari-

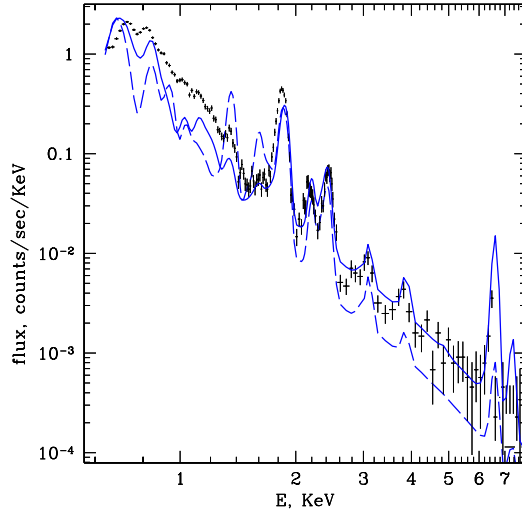


**Fig. 8.** X-ray spectra of the simulated and the observed (merged MOS1 and MOS1) remnants. The theoretical spectra are based on W7 ( $\chi^2/d.o.f. \approx 21$ , dashed line) and delayed-detonation c050403m ( $\chi^2/d.o.f. \approx 13$ , solid line) explosion models.  $\rho_{CSM} = 3 \times 10^{-25}$  g/cm<sup>3</sup>, age  $t = 400$  years,  $E_{CR}/E_g \approx 0.4$ .

son with real supernova remnants and more sophisticated schemes modeling them.

The value of the energy density found for relativistic particles  $E_{CR}$  can be used to estimate the intensity of magnetic field in the remnant. Assuming that  $E_{CR}$  and  $B^2/8\pi$  should be of the same order of magnitude, we derive  $B = 500 \pm 200 \mu G$ . This value appears to be somewhat high for this SNR, but still within reasonable limits. For example, using the correlation  $\rho_{CSM}v_s^3 \propto B^2$  from Vink (2006, Fig. 6) one might expect  $B \lesssim 100 \mu G$ .

The list of the typical properties of these models is also presented in Table 2. In this case the difference between electron and ion temperatures is not so drastic:  $T_e/T_i \approx 0.03$ , which is still in agreement with Ghavamian et al. (2000), where at  $\gamma = 4/3$  (relativistic equation of state) the SNR plasma velocities (of  $\sim 4500$  km/s) correspond to  $T_e/T_i \approx 10^{-2}$ .

## 5. Discussions and concluding remarks

The analysis of the XMM-Newton X-ray spectrum of the SNR 0509-67.5 allowed us to estimate basic parameters of the object and reveals several peculiar features.

First of all we obtained reasonable and consistent estimates for the CSM density, using various methods: the EPIC MOS data fitting gives the estimates of the circumstellar medium density of  $n_{CSM} \lesssim 0.6$  cm<sup>-3</sup>, the RGS spectral fitting of nitrogen abundance (which is not a product of thermonuclear explosion) yield  $n_{CSM} = 0.4 - 0.8$  cm<sup>-3</sup>. In the hydrodynamical simulations we



**Table 2.** Observed properties of the SNR 0509-67.5 and the properties of the numerical models: the one with the “basic” set up and one with a relativistic component (Eq.1). The table columns are: R – visible remnant’s radius (in the models this is the position of the contact discontinuity), t – the age,  $n_{\text{CSM}}$  – circumstellar number density,  $v$  – velocity of the shocked ejecta (maximum value for the numerical models),  $kT_e$  – electron temperature (for numerical models it is the maximum temperature),  $kT_i$  – maximum ion temperature,  $M_{\text{Fe}}$  – an estimate of the swept up iron mass (in solar masses),  $N_H$  – column density on the line of sight (derived from XSPEC, Arnaud 1996, spectral fitting).

Parameters	R, pc	t, yrs	$n_{\text{CSM}} \text{ cm}^{-3}$	$v$ , km/s	$kT_e$ , keV	$kT_i$ , keV	$M_{\text{Fe}}, M_{\odot}$	$N_H 10^{21} \text{ cm}^{-2}$
SNR 0509-67.5	3.6	$\lesssim 500$	0.4 – 0.6	$4900 \pm 400$	2.5 – 3.6	-	$\sim 0.05$	-
W7(basic)	3.6	400	0.1	$\lesssim 4600$	0.5 – 3.6	150 – 2500	$\sim 0.12$	$0.7 \pm 0.3$
c050403m(basic)	3.7	400	0.1	$\lesssim 4200$	1 – 1.5	30 – 40	$\sim 0.36$	$5.6 \pm 0.3$
W7(CR)	3.6	400	0.1	$\lesssim 4300$	1.8 – 1.9	20 – 36	$\sim 0.12$	$2.1 \pm 0.3$
c050403m(CR)	3.8	400	0.1	$\lesssim 4700$	2 – 45	30 – 300	$\sim 0.36$	$2.6 \pm 0.3$

have found similar, but somewhat lower value of  $n_{\text{CSM}} = 0.1 \text{ cm}^{-3}$ .

The abundances deduced from a single ionization timescale NEI (Fig.3) show that swept up amount of iron in the remnant is low. Moreover the model was unable to reproduce the observed Fe K line, so the line was fitted separately. The centroid of Fe K line is located at  $6.50 \pm 0.05 \text{ keV}$ , so it should be produced by low ionized ( $\leq \text{XVII}$ ) ions of iron. This could mean that the reverse shock of the remnant just recently reached and heated up the iron core of the supernova. The Fe K feature enables us to make a crude estimate of the amount of heated iron of  $M_{\text{Fe}} \sim 0.1 M_{\odot}$ .

In a framework of a NEI model with fixed single ionization timescale, abundances of the species lighter than aluminum tend to be overestimated, meanwhile, the amount of heavy species (iron group) tends to be underestimated (Hughes et al. 1998). For example, in the W7 model the Mg/Si line flux ratio is higher than observed (Fig.6, Fig.8), while Fig.3 shows that the Mg/Si abundance ratio is lower compared to the observed one. The same is true for the iron abundance: Badenes et al. (2008); Rest et al. (2008) showed that the remnant has a very large amount of iron, while the abundance of Fe, deduced from this simple fitting is considerably low. Note, however, that probably most of the Fe has not yet been heated by the reverse shock.

In this context (using only abundances derived from single ionization timescale NEI model) it is hard to determine the precise explosion mechanism. If we consider only the species from Si to Ar, then a delayed-detonation model with  $M_{\text{Fe}} = 0.9 M_{\odot}$  and an explosion energy of  $1.4 \times 10^{51} \text{ ergs}$  (Woosley et al. 2007) seems more preferable (Fig.3). The same tendency is confirmed by comparison of the observed spectra and the spectra from numerical simulations, performed in this study. This conclusion is in agreement with the results obtained by Badenes et al. (2008); Rest et al. (2008).

A separate study of the remnant’s bright southwest region shows that this spot appears to be more metal-rich: our fitting shows that it is at least twice more abundant in metals than the average metallicity throughout the remnant. This points to either an asymmetric explosion of the SNR or asymmetric CSM. Meanwhile note, that in Ghavamian et al. (2007) it was mentioned that this region has a blueshifted velocity excess. Which is a hint for an asymmetric explosion.

The numerical models are in agreement with the overall properties of SNR 0509-67.5 inferred from the studies presented in Section 3, which are as following: the CSM density  $\rho_{\text{CSM}} \simeq 3 \times 10^{-25} \text{ g/cm}^3$ , the age  $t = 350 - 400$  years, and the plasma velocities  $v \simeq 4000 - 5000 \text{ km/s}$ . The ratio of electron to ion temperatures of  $T_e/T_i \simeq 0.01$  is in satisfactory agreement with the expansion velocity of the remnant (Ghavamian et al. 2000), but heavily depends on the assumed explosion model (see also Badenes et al. 2006). Ejecta abundances govern electron population  $n_e$  and thus, the X-ray spectral shape. The latter is used to find the “best-fit” value of  $T_e/T_i$ .

The low value of  $T_e/T_i$  together with almost undetectable power-law emission point to the yet ineffective role of plasma instabilities and/or magnetic field at this stage in this object. Nevertheless, the simulations also indicate that the energy of relativistic particles is probably not negligible and may contribute up to  $\sim 40\%$  of thermal energy, so the magnetic field (provided that  $E_{\text{CR}} \sim B^2/8\pi$ ) might be slightly higher,  $\sim 500 \mu\text{G}$ , than the expected value of  $\sim 100 \mu\text{G}$  based on the relation reported by Vink (2006), but within reasonable limits.

We have found satisfactory hydrodynamical models for the remnant, but many problems still exist.

In our synthetic spectra some of the line centroids and line fluxes ratios do not perfectly fit the observations. This is partly due to limited set of explosion models available and to still appreciable number of free parameters (electron temperature, thermal conduction, magnetic fields,

cosmic ray particles, and other non-thermal and relativistic effects). For instance, more energetic explosion model ( $E > 1.4 \times 10^{51}$ ) could produce a supernova remnant at the age of 350 – 400 years with required high ejecta velocity, observed radius, and more acceptable higher value of CSM density (up to  $10^{-24}$  g/cm<sup>3</sup>). Nevertheless such a model should contain a lot of <sup>56</sup>Ni and small amount of Si and S. The X-ray spectra produced by such an explosion model disagree with the observed one which contains a very well pronounced Si K and S K lines.

Moreover, one of the shortcomings of the code is that for the calculation of the X-ray emission, and for the reproduction of the observed spectrum around 1 keV, we need to update the atomic data for Fe L code. A task that we plan to undertake in the near future.

To create more or less reliable models for supernova remnants, further developments of the physics in hydrodynamical simulations are required. Self-consistent treatment of cosmic-rays acceleration is necessary. 3D simulations may shed some light on the influence of various instabilities on the SNR dynamics. Further analysis of high resolution X-ray spectra is needed to evaluate the conditions in other SNRs as well.

*Acknowledgements.* We are grateful to the referee C. Badenes for valuable comments which helped to improve the paper. We also thank P. Lundqvist for providing his X-ray code which is incorporated in the package SUPREMNA, J. Kaastra for helpful advice on X-ray line emission issues, M. Gilfanov for valuable pointers to X-ray data sources and S. Woosley for his set of SN Ia models used in our work.

DK and JV are supported by a Vidi grant from the Netherlands Organization for Scientific Research (PI J. Vink), The work of DK is also partially supported in Russia by RFBR under grants 05-02-17480, 06-02-16025, 07-02-00961, and by Russian Leading Scientific School Foundation under grant RLSS-2977.2008.2.

SB is supported in Russia partly by grants RFBR 07-02-00830-a, RLSS-3884.2008.2 and by grant IB7320-110996/1 of the Swiss National Science Foundation.

## References

- Arnaud, K. 1996, in ASP Conf. Series volume 101 (Jacoby G. and Barnes J.), 17
- Badenes, C., Borkowski, K., Hughes, J., Hwang, U., & Bravo, E. 2006, *ApJ*, 645, 1373
- Badenes, C., Hughes, J. P., Bravo, E., & Langer, N. 2007, *ApJ*, 662, 472
- Badenes, C., Hughes, J. P., Cassam-Chenai, G., & Bravo, E. 2008, eprint arXiv:0801.4761
- Behar, E., Rasmussen, A. P., Griffiths, R. G., et al. 2001, *A&A*, 365, 242
- Berezhko, E. & Ellison, D. C. 1999, *ApJ*, 526, 385
- Blondin, J. M. & Ellison, D. C. 2001, *ApJ*, 560, 244
- Cassam-Chenaï, G., Decourchelle, A., Ballet, J., et al. 2004, *A&A*, 414, 545
- Cassam-Chenaï, G., Hughes, J. P., Ballet, J., & Decourchelle, A. 2006, *ApJ*, 665, 315
- Chevalier, R. A. 1983, *ApJ*, 272, 765
- de Plaa, J., Kaastra, J. S., Tamura, T., et al. 2004, *A&A*, 423, 4956
- den Herder, J. W., Brinkman, A. C., Kahn, S. M., Branduardi-Raymont, G., & Thomsen, K. e. a. 2001, *A&A*, 365, 7
- Gaetz, T. J. & Salpeter, E. E. 1983, *ApJS*, 52, 155
- Ghavamian, P., Blair, W. P., Sankrit, R., Raymond, J. C., & Hughes, J. P. 2007, *ApJ*, 664, 304
- Ghavamian, P., Laming, J. M., & Rakowski, C. E. 2000, *ApJ*, 654, 69
- Helder, E. & Vink, J. 2008, submitted to *ApJ*
- Hendrick, S. P. & Reynolds, S. 2001, *ApJ*, 559, 903
- Hughes, J. P., Hayashi, I., & Koyama, K. 1998, *ApJ*, 505, 732
- Iwamoto, K., Brachwitz, F., Nomoto, K., et al. 1999, *ApJS*, 125, 439
- Kaastra, J. & Mewe, R. 1993, *ApJS*, 97, 443
- Kaastra, J., Mewe, R., & Nieuwenhuijzen, H. 1996, in UV and X-ray spectroscopy of astrophysical and laboratory plasmas (K. Yamashita and T. Watanabe), 411
- Kosenko, D. 2006, *MNRAS*, 369, 1407
- Mewe, R., Gronenschild, E. H. B. M., & van den Oord, G. H. J. 1985, *A&AS*, 62, 197
- Nomoto, K., Thielemann, F.-K., & Yokoi, K. 1984, *ApJ*, 286, 644
- Rasmussen, A. P., Behar, E., Kahn, S. M., den Herder, J. W., & van der Heyden, K. 2001, *A&A*, 365, 231
- Rest, A., Matheson, T., Blondin, S., et al. 2008, eprint arXiv:0801.4762
- Rest, A., Suntzeff, N., & et al, K. O. 2005, *Nature*, 438, 1132
- Sasaki, M., Gaetz, T. J., Blair, W. P., et al. 2006, *ApJ*, 642, 260
- Sorokina, E., Blinnikov, S., Kosenko, D., & Lundqvist, P. 2004, *Astronomy Letters*, 30, 737
- Strüder, L., Briel, U., Dennerl, K., Hartmann, R., & Kendziorra, E. e. a. 2001, *A&A*, 365, 18
- Turner, M. J. L., Abbey, A., Arnaud, M., Balasini, M., & Barbera, M. e. a. 2001, *A&A*, 365, 27
- van der Heyden, K. J., Behar, E., Vink, J., et al. 2002, *A&A*, 392, 955
- van der Heyden, K. J., Bleeker, J. A. M., & Kaastra, J. S. 2004, *A&A*, 421, 1031
- van der Heyden, K. J., Paerels, F., Cottam, J., Kaastra, J. S., & Branduardi-Raymont, G. 2001, *A&A*, 365, 254
- Vink, J. 2006, in The X-ray Universe 2005 (San Lorenzo de El Escorial, Madrid, Spain (ESA SP-604)), eprint astro-ph/0601131
- Vink, J. & Laming, J. M. 2003, *ApJ*, 758, 584
- Vink, J., Laming, J. M., Gu, M. F., Rasmussen, A., & Kaastra, J. S. 2003, *ApJ*, 31, 587
- Warren, J. S. & Hughes, J. P. 2004, *ApJ*, 608, 261
- Warren, J. S., Hughes, J. P., Badenes, C., et al. 2005, *ApJ*, 634, 376
- Werner, N., de Plaa, J., Kaastra, J. S., et al. 2006, *A&A*, 449, 475
- Woosley, S. E., Kasen, D., Blinnikov, S., & Sorokina, E. 2007, *ApJ*, 662, 487